metals

MDPI

Article

Grain Refinement of AZ91 Magnesium Alloy Induced by Al-V-B Master Alloy

Wang Chang [1,2], Yanping Shen [1], Yueying Su [1], Long Zhao [1], Yunhu Zhang [1,2,*], Xiangru Chen [1], Ming Sun [3], Jichun Dai [4] and Qijie Zhai [1,2]

1 Center for Advanced Solidification Technology, Shanghai University, Shanghai 200072, China; changwangshu@163.com (W.C.); shenyp1102@163.com (Y.S.); yueyingSU@shu.edu.cn (Y.S.); zhaolongXYZ@shu.edu.cn (L.Z.); chenxr@shu.edu.cn (X.C.); qjzhai@shu.edu.cn (Q.Z.)
2 Materials Genome Institute of Shanghai University, Shanghai University, Shanghai 200072, China
3 School of Materials Science and Engineering, University of Shanghai for Science and Technology, Shanghai 200093, China; ssm@usst.edu.cn
4 Research Institute (R & D Center), Shanghai June Bang Technology Corporation, Shanghai 200032, China; jichun.dai@gmail.com
* Correspondence: zhangyunhu.zyh@163.com

Received: 12 November 2019; Accepted: 6 December 2019; Published: 10 December 2019

Abstract: It has long been recognized that grain refinement of Mg-Al alloys is difficult, although various methods have been tried. In the present paper, a novel grain refiner, Al-3.4V-1B master alloy, has been developed to refine the as-cast AZ91 alloy. A comparative study on grain refinement effects of Al-3.4V-1B, Al-5V, and Al-3Ti-1B master alloys was performed under the same solidification conditions. It is shown that Al-3.4V-1B master alloy not only has significant grain refinement ability, but also keeps stable anti-fading capacity with holding time up to 2 h. Based on the analysis of grain refinement, VB_2 particles introduced by Al-3.4V-1B master alloy are the heterogeneous nuclei for AZ91 alloy.

Keywords: grain refinement; AZ91; Al-V-B master alloy; heterogeneous nucleation

1. Introduction

Mg alloys are known as "green engineering materials for the 21st century", which have been used in aerospace, automobiles, electronic products due to their low densities, and high specific strengths [1–3]. With the increase in demands for energy conservation and emission reduction, light-weighting materials including Mg alloys will be in continuous demand [4,5]. Among all the Mg alloys, Mg-Al alloys have attracted much interest since the alloying element Al is of low in cost and effective in improving strength [6].

Grain refinement can not only simultaneously improve strength and ductility, but also can reduce casting defects, such as segregations and porosity. Zirconium has been widely applied to cause grain refinement of magnesium alloys. After adding 0.15 wt.% of zirconium to the melt, a grain size reduction of more than 80% was achieved [7]. However, the significant grain refinement induced by zirconium does not occur in these magnesium alloys with aluminum, because aluminum and zirconium can readily form stable intermetallic phases, which are unfortunately ineffective as nucleant particles for magnesium grains [7,8].

During the past decades, achieving grain refinement in Mg-Al alloys has been demonstrated to be an extremely difficult issue, although several methods have been developed including superheating [8,9], mechanical shearing [10], ultrasonic wave [11–13], electromagnetic fields [14,15], addition of solute elements [16–21], inoculations [22–28]. For instance, superheating applied on a commercial scale is

less practical owing to the requirement for rapid cooling from the treatment temperature to pouring temperature. Mechanical shearing, ultrasonic wave and electromagnetic fields cannot be directly applied to cause grain refinement in castings with complex geometry. The addition of solute elements may contaminate the melt or deteriorate physical properties. Carbon inoculation, such as using C_2Cl_6 and Al_4C_3 [24], can refine the grains of the Mg-Al alloys, but the use of C_2Cl_6 may cause environmental problems and the use of carbon may contaminate the alloys. However, more attention has been paid to the Mg-Al alloys inoculated by Al-Ti-B master alloy because the achieved grain refinement is more effective, easy, and reliable [7,23,25,29,30]. Wang et al. [30] reported that the grain size of AZ31 magnesium alloy can be effectively reduced by the optimal addition level of 0.3 wt.% Al-4Ti-5B master alloy and TiB_2 particles act as heterogeneous nuclei. Chen et al. [23] studied the effects of refining parameters on the grain size of AZ91D magnesium alloy using an Al-Ti-B master alloy. A process route was developed that 0.3% Al-Ti-B master alloy is added at a temperature of 750 °C, after holding 30 min the melt is cooled to 705 °C as quickly as possible and poured. However, when the holding time exceeds the given time, the TiB_2 particles will agglomerate and settle down, resulting in the decrease of effective substrate number and thus the increase of grain size. Therefore, effective grain refiner for Mg-Al alloy still needs to be developed.

In this paper, an alternative grain refiner for commercial AZ91 alloy, Al-V-B master alloy was prepared to study its grain refinement ability in comparison with the Al-Ti-B and Al-V master alloy. Furthermore, these potential heterogeneous nuclei were analyzed in detail. Since the finest grain size was achieved in the AZ91 alloy inoculated by Al-V-B refiner rather than the Al-Ti-B refiners, Al-V-B master alloy has a potential to be a grain refiner for AZ91 alloy.

2. Experimental Method

AZ91 alloy was employed as it is a widely used Mg-Al alloy. The Al-3.4V-1B master alloy was prepared from the commercial Al-5V and Al-3B master alloy (Sichuan Lande Industry Company Ltd. Chengdu, China) with the weight ratio of 2:1 in a graphite crucible. Commercial Al-3Ti-1B master alloy was also employed for comparisons. The chemical compositions of the AZ91 alloy, Al-3.4V-1B, Al-3Ti-1B, and Al-5V master alloy were determined by ICP-AES (Optima 7300DV, PerkinElmer, MA, USA) and listed in Table 1.

Table 1. Chemical compositions of the employed alloys.

Alloys	**Element (wt.%)**								
AZ91	Al	Zn	Mn	Si	Fe	Cu	Ni	Be	Mg
(wt.%)	8.94	0.57	0.21	0.022	0.0033	0.0022	0.0009	0.0009	Balance
Al-3Ti-1B	Ti	B	Fe	Si	Mn			Al	
(wt.%)	3.13	0.93	0.06	0.06	<0.01			Balance	
Al-3.4V-1B	V	B	Fe	Zn	Cu			Al	
(wt.%)	3.17	1.09	0.07	<0.01	0.01			Balance	
Al-5V	V	Si	Fe	Ti	B			Al	
(wt.%)	5.11	0.10	0.14	<0.03	<0.01			Balance	
Al-3B	B	Fe	Si	Cu	Zn	Na		Al	
(wt.%)	3.07	0.15	0.08	<0.03	<0.04	<0.50		Balance	

Schematic view of solidification setup is shown in Figure 1. Approximate 2 kg of commercial AZ91 alloy was re-melted in a mild steel crucible in an electrical furnace (SG2-3-10, Shanghai Shiyan Electric Furnace Company Ltd. Shanghai, China) under a protecting gas (0.3% SF_6 and 99.7% CO_2) at 973 K for 2 h. All samples were obtained through scooping the top melt by a conical steel mold (Ø50 mm × Ø20 mm × h50 mm). In order to avoid the contamination by Fe element, the crucible and the mold were coated by a layer of coating composed of 30 wt.% French chalk, 5 wt.% sodium silicate, and 65 wt.% water. Then, the melt was inoculated by 0.6 wt.% of the master alloy at the temperature of

973 K, and mechanically stirred for homogenization. After respective holding times of 10, 30, 60, 90, and 120 min, five inoculated AZ91 samples were taken out for each of the holding times from the melt using the mold and cooled under protective gas. It is well known that the MgF_2 can form on the free surface of Mg alloy melt to prevent burning when SF_6 gas is flowed on the free surface. However, SF_6 is harmful to the environment and is expensive. Therefore, a mixture gas with an optimal ratio of 0.3% SF_6 and 99.7% CO_2 was employed as the protective gas in this study. The cooling curve was monitored by a temperature acquisition system (YADU700R, Shanghai Yadu Instrument, Shanghai, China) with a frequency of 10 data points per second and accuracy of ±0.1 °C. K-type thermocouple with diameter of 0.5 mm was employed and located at the center of ingot. The pre-solidification cooling rate of about 1 °C/s was calculated from cooling curves among the temperature range of 700 °C to 592 °C. More details can be found in reference [31].

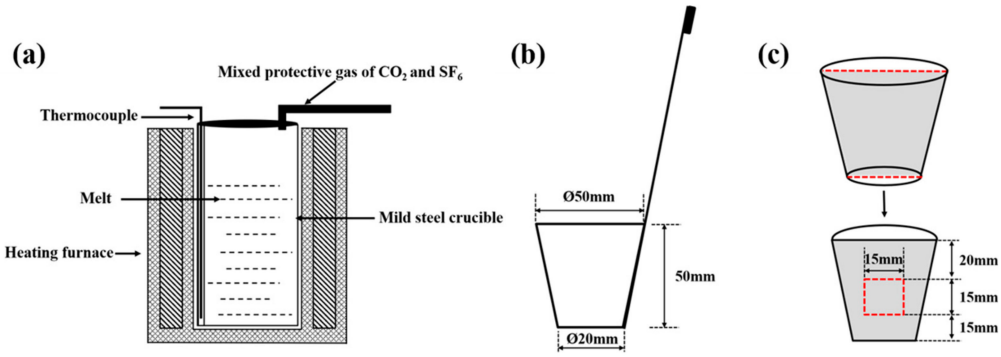

Figure 1. Schematic views of (**a**) solidification setup, (**b**) cone mold, and (**c**) sample cutting.

Solidified ingots were sectioned longitudinally along the mid-plane. Then, specimens with size of 15 mm × 15 mm were machined from the sectioned samples above the bottom 15 mm (see Figure 1c). Prepared specimens were ground and polished by standard metallographic technique. In order to quantitatively examine the grain size, these specimens were etched by one etchant (composed of 4.2 g of picric acid, 70 mL of absolute ethanol, 10 mL of acetic acid, and 10 mL of distilled water) for 10 s, and then etched by another etchant (composed of 150 mL of absolute ethanol, 50 mL of distilled water, and 1 mL of acetic acid) for about 75 s. The etched specimens were observed using a Zeiss optical microscope (Axio Imager.A2m, ZEISS, Oberkochen, Germany) under polarized light. The grain size was measured from the optical images by using linear intercept methods according to ASTME112-96. As for the grain size measurement, 5 areas were randomly selected from each as-cast sample. According to the measured 5 grain size for each sample, the standard deviation was calculated as the error of grain size. The microstructure was observed using Phenom scanning electron microscope (SEM, Phenom ProX, Phenom, Eindhoven, Netherland). Element mapping were carried out using an electron probe microanalyzer (EPMA-8050G, Shimadzu, Kyoto, Japan). The phase identification was performed using means of Bruker X-ray diffraction (XRD, D2 PHASER, Bruker, Karlsruhe, Germany) Analyzer.

3. Results

3.1. Characteristics of Al-3.4V-1B and Al-5V Master Alloys

Figure 2 gives the XRD pattern of Al-3.4V-1B and Al-5V master alloys. It displays that the Al-3.4V-1B master alloy consists of α-Al, Al_3V, and VB_2 phases, whereas the α-Al and Al_3V phases appear in the Al-5V master alloy.

Figure 3 shows the microstructures of Al-3.4V-1B master alloy. As the back-scattered electron image shown in Figure 3a, it consists of gray matrix, large-sized polygonal white particles with size of about 10–20 μm, and small-sized white particles with size range from hundreds of nanometers to a few microns. Figure 3b–d displays the Energy Dispersive Spectroscopy (EDS) mapping of Al, V, and B elements in the Al-V-B master alloy, respectively. Since the highest Al content is observed in the gray

matrix, it is no doubt that the matrix is the α-Al phase. V and Al elements appears in the large-sized particles, whereas the small-sized white particles possess V and B elements. According to the XRD results shown in Figure 2, it can be concluded that the large and small particles are corresponding to Al_3V and VB_2 metallic compounds, respectively.

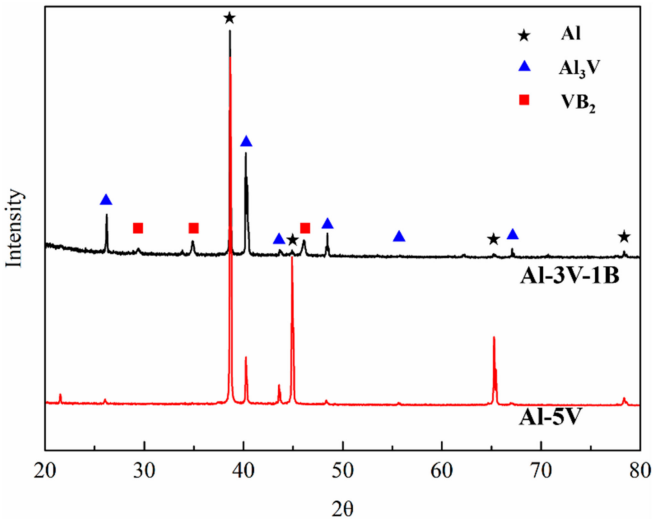

Figure 2. XRD of Al-3.4V-1B and Al-5V master alloys.

Figure 4 shows the microstructures and elements mapping of Al-5V master alloy. As shown in Figure 4a, coarse dendrite white phase is embedded in gray matrix. As the Al and V element mapping shown in Figure 4b,c, V and Al elements appear in the dendrite white phase, while only Al element is observed in the gray matrix. According to the corresponding XRD of the Al-5V master alloy shown in Figure 2, it is no doubt that the dendrite white phase is Al_3V metallic compound, which are surrounded by the α-Al matrix.

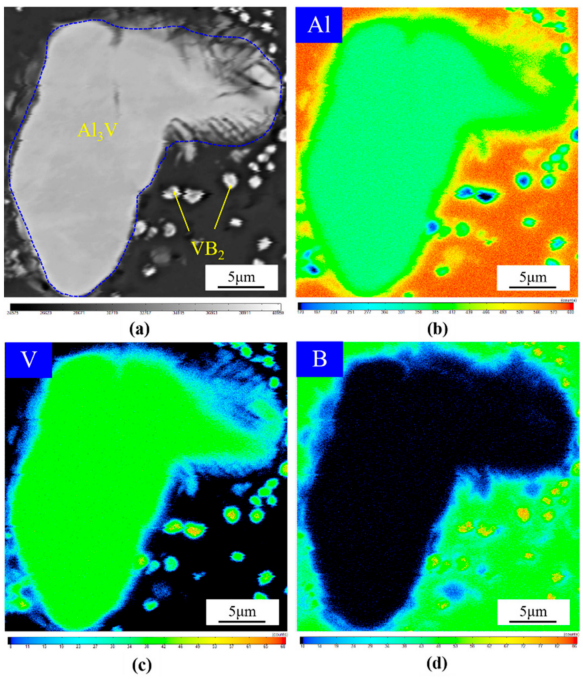

Figure 3. Microstructures and elemental mapping of Al-3.4V-1B master alloy: (**a**) microstructures, (**b**) Al element, (**c**) V element, and (**d**) B element.

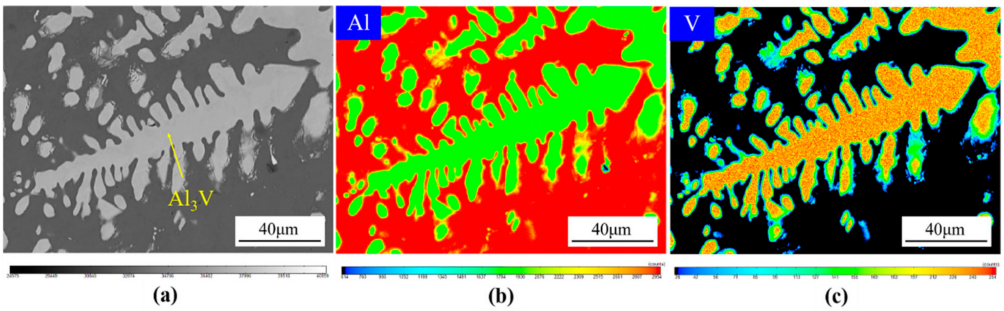

Figure 4. Microstructures and elemental mapping of Al-5V master alloy: (**a**) microstructures, (**b**) Al element, and (**c**) V element.

3.2. Grain Refining Performance of the Al-3.4V-1B Master Alloy

In order to give a reference, Figure 5 presents the solidified microstructures of the AZ91 alloy without inoculation. It can be seen that AZ91 alloy without inoculation has coarse microstructure with an average grain size about 1156 μm (±114 μm). Figure 6 shows the solidified microstructures of AZ91 alloy inoculated by Al-3.4V-1B, Al-3Ti-1B, and Al-5V master alloys after holding times of 10, 60, and 120 min, respectively. Correspondingly, Figure 7 plots the variations in grain size as a function of holding time for AZ91 alloy inoculated by Al-3.4V-1B, Al-3Ti-1B, and Al-5V master alloys, respectively. As shown in Figure 6a, significant grain refinement is achieved in AZ91 alloy inoculated by Al-3.4V-1B master alloy. The quantitatively measured results display that the grain size of the AZ91 alloy refined by Al-3.4V-1B refiner is obviously less than that of the reference sample and the samples inoculated by Al-3Ti-1B and Al-5V master alloy (see Figure 7). It indicates that the Al-3.4V-1B master alloy can efficiently refine the AZ91 alloy than that of Al-3Ti-1B and Al-5V master alloy.

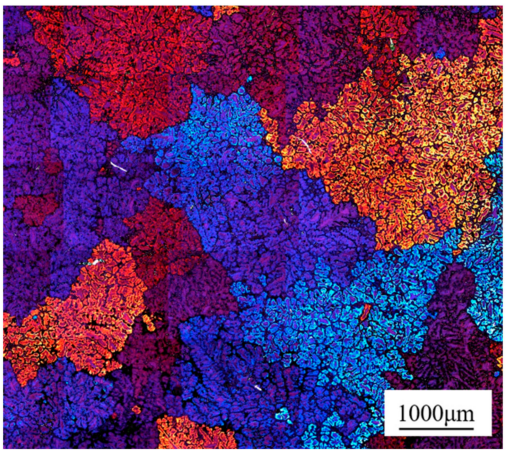

Figure 5. Solidified structures of AZ91 alloy without inoculation.

In addition, as shown in Figure 6a, no obvious variations in grain size are observed in Al-3.4V-1B inoculated AZ91 alloy with the increase of holding time (even to 2 h). Figure 6b shows that the grain size is refined by the Al-3Ti-1B master alloy. However, when the holding time exceeds 30 min, the refining effect of Al-3Ti-1B alloy is gradually faded with the increase of holding time. Especially when the holding time reached 90 min, the grain size was comparable to that of the unrefined AZ91 alloy. This phenomenon is consistent with the previous investigations [23]. Similarly, the fading of grain refinement ability of Al-5V master alloy for AZ91 alloy is also revealed in Figure 6c. As the holding time increased, the grain size variation of the sample inoculated by Al-3.4V-1B maser alloy is among the range of 466 μm (±27 μm) to 600 μm (±36 μm), whereas the grain size of AZ91 alloy with addition of Al-3Ti-1B and Al-5V master alloy is correspondingly increased from 677 μm (±47 μm) to 1388 μm (±54 μm) and from 1129 μm (±97 μm) to 1416 μm (±79 μm), respectively. It suggests that the Al-3.4V-1B

master alloy has the potential to be fading resistance (anti-fading) refiner for AZ91 alloy compared with Al-3Ti-1B and Al-5V master alloys.

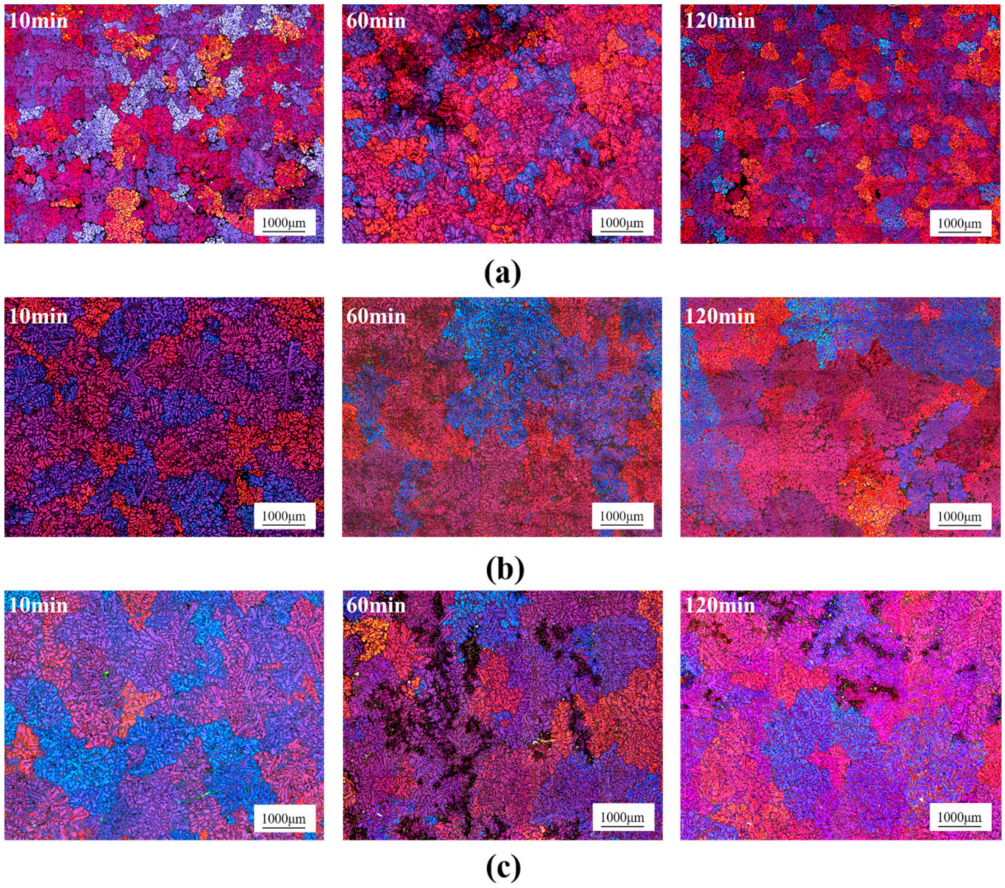

Figure 6. Solidified structures of the AZ91 alloys inoculated by master alloys after different holding times: (**a**) Al-3.4V-1B, (**b**) Al-3Ti-1B, and (**c**) Al-5V.

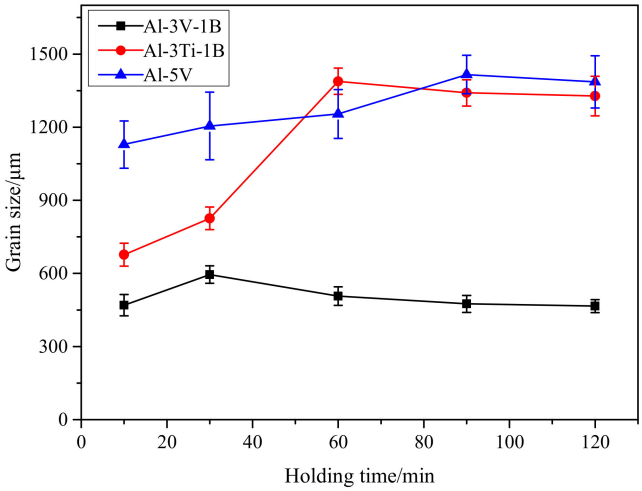

Figure 7. Variation in grain size of AZ91 alloy inoculated by different master alloys.

4. Discussion

The results shown in Figures 6 and 7 present that significant grain refinement is achieved in the AZ91 alloy inoculated by Al-3.4V-1B master alloy. Figures 3 and 4 display that the VB_2 metallic compound is formed in Al-3.4V-1B master alloy besides Al_3V particles which is the only observed

metallic compound in Al-5V master alloy. It is most likely that the VB_2 particles are the potential effective nucleation sites for AZ91 alloy rather than Al_3V particles due to the fact that the no obvious grain refinement is obtained in AZ91 alloy inoculated by Al-5V master alloy.

Figure 8 shows solidified microstructures and element mapping of the AZ91 alloy refined with Al-3.4V-1B master alloy. As shown in Figure 8a, three phases are surrounded by primary Mg matrix. According to the element mapping (see Figure 8b–f) and previous literatures [19,23,28,32], it can be deduced that the coarse irregular phase, white polygon particles, and small concentrated particles are $Mg_{17}Al_{12}$, Al_8Mn_5, and VB_2 intermetallic compound, respectively. Although it can be observed that some VB_2 particles are surrounded by $Mg_{17}Al_{12}$ phase, the isolated VB_2 particles embedded in primary Mg matrix still can be found. In addition, it should be noted that although most of the VB_2 particles are concentrated as clusters, the dispersed individual VB_2 particles are presented as shown in Figure 8a. The previous studies prove that Al_8Mn_5 particle is not heterogeneous nucleus in magnesium alloys [33]. Therefore, VB_2 particles can act as the heterogeneous nuclei to refine the AZ91 alloy grains.

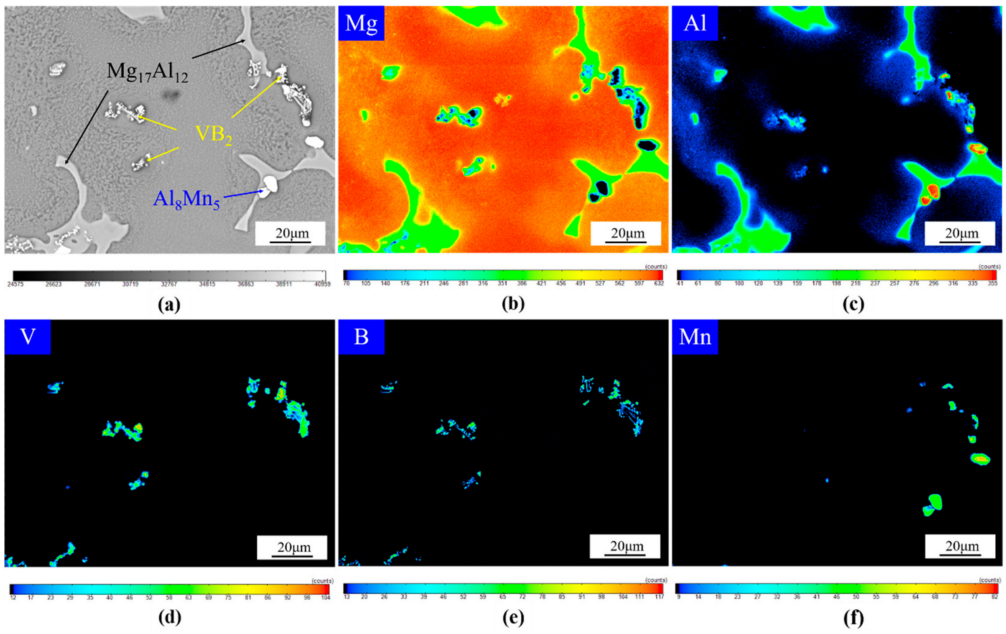

Figure 8. Microstructures and elemental mapping of AZ91 alloy: (**a**) microstructures, (**b**) Mg element, (**c**) Al element, (**d**) V element, (**e**) B element, and (**f**) Mn element.

It is well known that the lattice misfit between nucleated phase and substrate can predict the nucleation potency of potent nuclei in bulk melt during solidification process. Bramfitt proposed a model by considering two-dimensional lattices misfit [34], which is calculated by Equation (1):

$$\delta_{(hkl)_n}^{(hkl)_s} = \sum_{i=1}^{3} \frac{\frac{\left| d_{[uvw]_s^i} \cos\theta - d_{[uvw]_n^i} \right|}{d_{[uvw]_n^i}}}{3} \tag{1}$$

where $d_{[uvw]_s^i}$ is the substrates' atomic spacing, $d_{[uvw]_n^i}$ is the nucleation-phase atomic spacing, θ is the angle between $d_{[uvw]_s^i}$ and $d_{[uvw]_n^i}$. This model also predicts that the maximum misfit of the effective substrate for nucleation phase is defined as 6% [8].

Our previous studies [35–37], with respect to the heterogeneous nucleation of Al/Au droplets on $MgAl_2O_4$, MgO, and Al_2O_3 substrates, have shown that the calculated minimum Bramfitt misfits may be a good indicator for the nucleation ability and the related orientation relationship between the potent nuclei and nucleated phase, which has been confirmed by the corresponding DSC experiments and TEM analysis. The crystal structure of VB_2, TiB_2, Mg, Al_3V, and Al_3Ti are shown in Table 2. The

respective minimum Bramfitt misfits between Mg and VB_2, Al_3V, TiB_2, Al_3Ti substrates are calculated as shown in Table 3. The value of misfit between Mg and VB_2 is much smaller than that between Mg and Al_3V, which is one of the reasons that the coarser solidified structures are generated in AZ91 alloy inoculated by Al-5V master alloy. Moreover, it should be noted here that the minimum Bramfitt misfit of Mg/VB_2 is 3%, which means that the VB_2 is a potent effective heterogeneous nuclei for Mg alloy because the maximum misfit of the effective substrate for nucleation phase is defined as 6% according to the literature [7].

Table 2. The crystal structure of Mg, VB_2, TiB_2, Al_3V, and Al_3Ti.

Phases	Crystal Structure	Lattice Constant	
Mg	hexagonal	a = 0.321 nm	c = 0.521 nm
VB_2	hexagonal	a = 0.2998 nm	c = 0.3057 nm
TiB_2	hexagonal	a = 0.3028 nm	c = 0.3228 nm
Al_3V	tetragonal	a = 0.3775 nm	c = 0.832 nm
Al_3Ti	tetragonal	a = 0.3854 nm	c = 0.8584 nm

Table 3. The misfit between VB_2, Al_3V, TiB_2, Al_3Ti, and Mg matrix under possible crystallographic orientation relationships.

Phases	Possible Crystallographic Orientation		
	$(0001)VB_2 \| (10\bar{1}0)Mg$		
$[UVW]VB_2$	[100]	$[\bar{2}10]$	$[\bar{2}00]$
[UVW]Mg	[010]	[001]	[011]
δ		3.0%	
	$(001)Al_3V \| (10\bar{1}0)Mg$		
$[UVW]Al_3V$	[010]	$[\bar{1}00]$	$[\bar{1}10]$
[UVW]Mg	[010]	[001]	[011]
δ		20.1%	
	$(0001)TiB_2 \| (10\bar{1}0)Mg$		
[UVW] TiB_2	[100]	$[\bar{2}10]$	$[\bar{2}00]$
[UVW]Mg	[010]	[001]	[011]
δ		2.46%	
	$(001)Al_3Ti \| (10\bar{1}0)Mg$		
$[UVW]Al_3Ti$	[010]	$[\bar{1}00]$	$[\bar{1}10]$
[UVW]Mg	[010]	[001]	[011]
δ		19.8%	

Although the calculated minimum Bramfitt misfit of Mg/TiB_2 is less than that of Mg/VB_2 as shown in Table 3, the grain size of AZ91 alloy inoculated Al-3Ti-1B master alloy is still larger than that of sample with Al-3.4V-1B master alloy. In addition, the solidified structure in the AZ91 alloy inoculated by Al-3Ti-1B master alloy gradually becomes coarser with the increase of holding time. It means that the grain refinement fading is generated. This is consistent with the results reported by T.J Chen [23]. It is proposed that the TiB_2 particles would agglomerate and settle down, resulting in the decrease of substrate number and thus the increase of grain size, when the holding time exceeds a given time. In contrast, since the significant grain refinement is steadily obtained in the AZ91 alloy inoculated by Al-3.4V-1B master alloy even though the holding time is as long as 120 min, it is most likely that the Al-3.4V-1B master alloy has a potential to be fading resistance grain refiner for AZ91 alloy.

In order to give more insights into this phenomenon, the microstructures of Al-3Ti-1B and Al-3.4V-1B master alloy have been compared as shown in Figure 9. It can be seen that TiB_2 particles in the Al-3Ti-1B master alloy tend to concentrate as clusters as shown in Figure 9a, while a mass of individual VB_2 particles can be found in the Al-3.4V-1B master alloy as shown in Figure 9b. Therefore,

the aggregation of TiB_2 particles may reduce the amount of heterogeneous nucleation sites, eventually resulting in lager grain size.

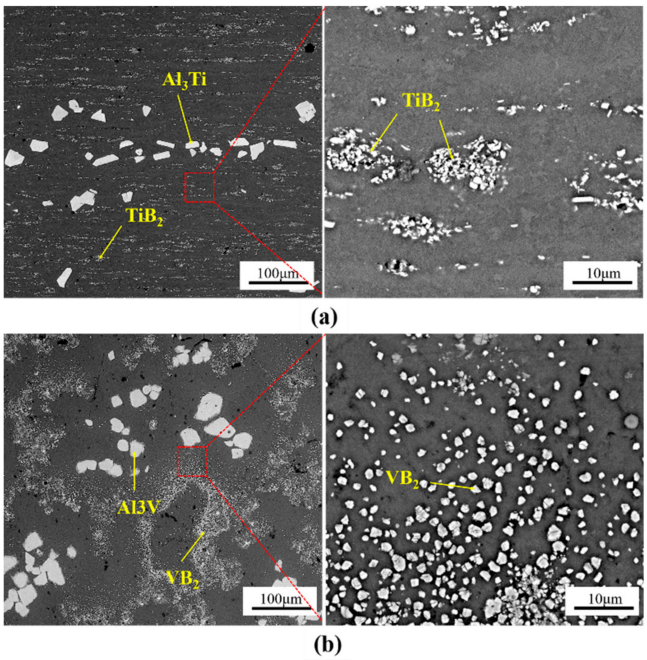

Figure 9. Microstructures of (**a**) Al_3Ti and TiB_2 particles in the Al-3Ti-1B master alloy and (**b**) Al_3V and VB_2 particles in the Al-3.4V-1B master alloy.

In addition, according to the Stokesx law [38], the sedimentation velocity (V) of the potential heterogeneous nucleation substrates inside the AZ91 liquid can be given by Equation (2):

$$V = \frac{\Phi^2 \cdot g \cdot \left(\rho_{sub} - \rho_{liq}\right)}{18 \cdot \eta} \tag{2}$$

where Φ is the diameter of the substrates, g is the gravitational acceleration, ρ_{sub} and ρ_{liq} are the density of the substrates and molten AZ91, respectively, and η is the viscosity of AZ91 melt. The density of TiB_2 (4.52 g/cm^3) is slightly smaller than that of VB_2 (5.1 g/cm^3). However, since the size of formed TiB_2 clusters is far larger than that of VB_2 particles, the sedimentation velocity of TiB_2 clusters would be much faster than that of VB_2 particles according to Equation (2). This is the possible reason why the Al-3.4V-1B master alloy anti-fading ability is better than the Al-3Ti-1B master alloy.

5. Conclusions

The grain refinement of AZ91 alloy induced by Al-3.4V-1B master alloy was investigated in the present paper.

(1) Significant grain refinement was achieved in the AZ91 alloy inoculated by Al-3.4V-1B master alloy. The grain size is decreased from 1156 μm (±114 μm) to 466 μm (±27 μm) with 0.6 wt.% addition of Al-3.4V-1B refiner. This represent a decrease of 60% in grain size.
(2) Al-3.4V-1B master alloy has a potential to be a fading resistance grain refiner for AZ91 alloy. This may be due to the more homogenized distribution of VB_2 particles in matrix and slower sedimentation rate in AZ91 melt.
(3) It is most likely that VB_2 particles are the effective nuclei for the grain refinement of AZ91 alloy inoculated by Al-3.4V-1B master alloy.

Author Contributions: Y.Z., M.S., and Q.Z. conceived and designed the experiments; W.C., Y.S. (Yanping Shen), and Y.S. (Yueying Su) performed the solidification experiments and grain size measurements; W.C., L.Z., X.C., and J.D. analyzed the results and fostered the interpretation; W.C., Y.Z., and M.S. wrote and revised the manuscript.

Funding: This research was funded by National Natural Science Foundation of China grant number 51974183, 51704192, 51320105003, and Shanghai Sailing Program grant number 17YF1405600.

Conflicts of Interest: The authors declare that they have no conflict of interest.

References

1. Mordike, B.; Ebert, T. Magnesium: Properties—Applications—Potential. *Mater. Sci. Eng. A* **2001**, *302*, 37–45. [CrossRef]
2. Dieringa, H. Influence of cryogenic temperatures on the microstructure and mechanical properties of magnesium alloys: A review. *Metals* **2017**, *7*, 38. [CrossRef]
3. Karakulak, E. A review: Past, present and future of grain refining of magnesium castings. *J. Magn. Alloy.* **2019**, *7*, 355–369. [CrossRef]
4. Friedrich, H.; Schumann, S. Research for a "new age of magnesium" in the automotive industry. *J. Mater. Process. Technol.* **2001**, *117*, 276–281. [CrossRef]
5. Hanko, G.; Antrekowitsch, H.; Ebner, P. Recycling automotive magnesium scrap. *JOM* **2002**, *54*, 51–54. [CrossRef]
6. Dahle, A.K.; Lee, Y.C.; Nave, M.D.; Schaffer, P.L.; StJohn, D.H. Development of the as-cast microstructure in magnesium–Aluminium alloys. *J. Light Metals* **2001**, *1*, 61–72. [CrossRef]
7. Ali, Y.; Qiu, D.; Jiang, B.; Pan, F.; Zhang, M.X. Current research progress in grain refinement of cast magnesium alloys: A review article. *J. Alloys Compd.* **2015**, *619*, 639–651. [CrossRef]
8. StJohn, D.H.; Qian, M.; Easton, M.A.; Cao, P.; Hildebrand, Z. Grain refinement of magnesium alloys. *Metall. Mater. Trans. A* **2005**, *36*, 1669–1679. [CrossRef]
9. Motegi, T. Grain-refining mechanisms of superheat-treatment of and carbon addition to Mg–Al–Zn alloys. *Mater. Sci. Eng. A* **2005**, *413*, 408–411. [CrossRef]
10. Men, H.; Jiang, B.; Fan, Z. Mechanisms of grain refinement by intensive shearing of AZ91 alloy melt. *Acta Mater.* **2010**, *58*, 6526–6534. [CrossRef]
11. Ramirez, A.; Qian, M.; Davis, B.; Wilks, T.; StJohn, D.H. Potency of high-intensity ultrasonic treatment for grain refinement of magnesium alloys. *Scr. Mater.* **2008**, *59*, 19–22. [CrossRef]
12. Aghayani, M.K.; Niroumand, B. Effects of ultrasonic treatment on microstructure and tensile strength of AZ91 magnesium alloy. *J. Alloys Compd.* **2011**, *509*, 114–122. [CrossRef]
13. Ferguson, J.; Schultz, B.; Cho, K.; Rohatgi, K.R. Correlation vs. causation: The effects of ultrasonic melt treatment on cast metal grain size. *Metals* **2014**, *4*, 477–489. [CrossRef]
14. Wang, Y.; Zeng, X.; Ding, W.; Luo, A.A.; Sachdev, A.K. Grain refinement of AZ31 magnesium alloy by titanium and low-frequency electromagnetic casting. *Metall. Mater. Trans. A* **2007**, *38*, 1358–1366. [CrossRef]
15. Sun, J.; Sheng, C.; Wang, D.P.; Zhang, Y.H.; Zhong, H.G.; Xu, Z.S.; Li, L.J.; Zhai, Q.J. Influence of pulsed magneto-oscillation on microstructure and mechanical property of rectangular 65Mn steel ingot. *J. Iron Steel Res. Int.* **2018**, *25*, 862–866. [CrossRef]
16. Lee, Y.; Dahle, A.; StJohn, D. The role of solute in grain refinement of magnesium. *Metal. Mater. Trans. A* **2000**, *31*, 2895–2906. [CrossRef]
17. Hirai, K.; Somekawa, H.; Takigawa, Y.; Higashi, K. Effects of Ca and Sr addition on mechanical properties of a cast AZ91 magnesium alloy at room and elevated temperature. *Mater. Sci. Eng. A* **2005**, *403*, 276–280. [CrossRef]
18. Li, S.S.; Tang, B.; Zeng, D.B. Effects and mechanism of Ca on refinement of AZ91D alloy. *J. Alloys Compd.* **2007**, *437*, 317–321. [CrossRef]
19. Suresh, M.; Srinivasan, A.; Ravi, K.; Pillai, U.; Pai, B. Influence of boron addition on the grain refinement and mechanical properties of AZ91 Mg alloy. *Mater. Sci. Eng. A* **2009**, *525*, 207–210. [CrossRef]
20. Zhang, J.; Wang, J.; Qiu, X.; Zhang, D.; Tian, Z.; Niu, X.; Tang, D.; Meng, J. Effect of Nd on the microstructure, mechanical properties and corrosion behavior of die-cast Mg–4Al-based alloy. *J. Alloys Compd.* **2008**, *464*, 556–564. [CrossRef]

21. Wang, J.; Li, X.B. Simultaneously improving strength and ductility of AZ91-type alloys with minor Gd addition. *J. Alloys Compd.* **2019**, *803*, 689–699. [CrossRef]
22. Guang, H.; Xiangfa, L.; Haimin, D. Grain refinement of Mg–Al based alloys by a new Al–C master alloy. *J. Alloys Compd.* **2009**, *467*, 202–207. [CrossRef]
23. Chen, T.; Wang, R.; Ma, Y.; Hao, Y. Grain refinement of AZ91D magnesium alloy by Al–Ti–B master alloy and its effect on mechanical properties. *Mater. Des.* **2012**, *34*, 637–648. [CrossRef]
24. Qian, M.; Cao, P. Discussions on grain refinement of magnesium alloys by carbon inoculation. *Scr. Mater.* **2005**, *52*, 415–419. [CrossRef]
25. Zhang, Q.; Liu, B.; Niu, Z.; Zhang, Z.; Leng, Z. Grain refinement and mechanical properties of Mg–5Li–3Al alloy inoculated by Al–5Ti–1B master alloy. *Mater. Sci. Eng. A* **2014**, *619*, 152–157. [CrossRef]
26. Guolong, M.; Guang, H.; Xiangfa, L. Grain refining efficiency of a new Al–1B–0.6 C master alloy on AZ63 magnesium alloy. *J. Alloys Compd.* **2010**, *491*, 165–169. [CrossRef]
27. Xiao, P.; Gao, Y.; Yang, X.; Xu, F.; Yang, C.; Li, B.; Li, Y.; Liu, Z.; Zheng, Q. Processing, microstructure and ageing behavior of in-situ submicron TiB_2 particles reinforced AZ91 Mg matrix composites. *J. Alloys Compd.* **2018**, *764*, 96–106. [CrossRef]
28. Xiao, P.; Gao, Y.; Xu, F.; Yang, S.; Li, B.; Li, Y.; Huang, Z.; Zheng, Q. An investigation on grain refinement mechanism of TiB_2 particulate reinforced AZ91 composites and its effect on mechanical properties. *J. Alloys Compd.* **2019**, *780*, 237–244. [CrossRef]
29. Koltygin, A.; Bazhenov, V.; Mahmadiyorov, U. Influence of Al–5Ti–1B master alloy addition on the grain size of AZ91 alloy. *J. Magnes. Alloys.* **2017**, *5*, 313–319. [CrossRef]
30. Wang, Y.; Zeng, X.; Ding, W. Effect of Al–4Ti–5B master alloy on the grain refinement of AZ31 magnesium alloy. *Scr. Mater.* **2006**, *54*, 269–273. [CrossRef]
31. Sun, M.; StJohn, D.H.; Easton, M.A.; Wang, K.; Ni, J.J. Effect of Cooling Rate on the Grain Refinement of Mg-Y-Zr Alloys. *Metal. Mater. Trans. A* **2019**, 1–5. [CrossRef]
32. Dini, H.; Andersson, N.E.; Jarfors, E.W. Effect of $Mg_{17}Al_{12}$ fraction on mechanical properties of Mg-9% Al-1% Zn cast alloy. *Metals* **2016**, *6*, 251. [CrossRef]
33. Wang, Y.; Xia, M.; Fan, Z.; Zhou, X.; Thompson, G. The effect of Al_8Mn_5 intermetallic particles on grain size of as-cast Mg–Al–Zn AZ91D alloy. *Intermetallics* **2010**, *18*, 1683–1689. [CrossRef]
34. Bramfitt, B.L. The effect of carbide and nitride additions on the heterogeneous nucleation behavior of liquid iron. *Metal. Trans.* **1970**, *1*, 1987–1995. [CrossRef]
35. Sun, J.; Wang, D.P.; Zhang, Y.H.; Sheng, C.; Dargusch, M.; Wang, G.; St John, D.; Zhai, Q.J. Heterogeneous nucleation of pure Al on MgO single crystal substrate accompanied by a $MgAl_2O_4$ buffer layer. *J. Alloys Compd.* **2018**, *753*, 543–550. [CrossRef]
36. Sheng, C.; Sun, J.; Wang, D.P.; Zhang, Y.H.; Li, L.J.; Chen, X.R.; Zhong, H.G.; Zhai, Q.J. Heterogeneous nucleation of pure gold on highly smooth ceramic substrates and the influence of lattice misfit and cooling rate. *J. Mater. Sci.* **2018**, *53*, 4612–4622. [CrossRef]
37. Wang, D.; Chang, W.; Shen, Y.; Sun, J.; Sheng, C.; Zhang, Y.H.; Zhai, Q.J. The role of lattice mismatch in heterogeneous nucleation of pure Al on Al_2O_3 single-crystal substrates with different termination planes. *J. Therm. Anal. Calorim.* **2019**, *137*, 1–7. [CrossRef]
38. Bolzoni, L.; Nowak, M.; Babu, N.H. On the effect of Nb-based compounds on the microstructure of Al–12Si alloy. *Mater. Chem. Phys.* **2015**, *162*, 340–345. [CrossRef]